Polymeric nanofiber coating with tunable combinatorial antibiotic delivery prevents biofilm-associated infection in vivo

Alyssa G. Ashbaugh[a,1], Xuesong Jiang[b,c,d,1], Jesse Zheng[e], Andrew S. Tsai[e], Woo-Shin Kim[a], John M. Thompson[f], Robert J. Miller[a], Jonathan H. Shahbazian[a], Yu Wang[a], Carly A. Dillen[a], Alvaro A. Ordonez[g,h], Yong S. Chang[g,h], Sanjay K. Jain[g,h], Lynne C. Jones[f], Robert S. Sterling[f], Hai-Quan Mao[b,c,d,i,2,3], and Lloyd S. Miller[a,b,f,j,2,3]

[a]Department of Dermatology, The Johns Hopkins University School of Medicine, Baltimore, MD 21231; [b]Department of Materials Science and Engineering, Johns Hopkins University, Baltimore, MD 21218; [c]Translational Tissue Engineering Center, Johns Hopkins University, Baltimore, MD 21218; [d]Institute for NanoBioTechnology, Johns Hopkins University, Baltimore, MD 21218; [e]Department of Biomedical Engineering, Johns Hopkins University, Baltimore, MD 21218; [f]Department of Orthopaedic Surgery, The Johns Hopkins University School of Medicine, Baltimore, MD 21287; [g]Department of Pediatrics, The Johns Hopkins University School of Medicine, Baltimore, MD 21287; [h]Center for Infection and Inflammation Imaging Research, The Johns Hopkins University School of Medicine, Baltimore, MD 21287; [i]Whitaker Biomedical Engineering Institute, Johns Hopkins University, Baltimore, MD 21218; and [j]Division of Infectious Diseases, Department of Medicine, The Johns Hopkins University School of Medicine, Baltimore, MD 21287

Edited by Scott J. Hultgren, Washington University School of Medicine, St. Louis, MO, and approved September 20, 2016 (received for review August 23, 2016)

Bacterial biofilm formation is a major complication of implantable medical devices that results in therapeutically challenging chronic infections, especially in cases involving antibiotic-resistant bacteria. As an approach to prevent these infections, an electrospun composite coating comprised of poly(lactic-coglycolic acid) (PLGA) nanofibers embedded in a poly(ε-caprolactone) (PCL) film was developed to locally codeliver combinatorial antibiotics from the implant surface. The release of each antibiotic could be adjusted by loading each drug into the different polymers or by varying PLGA:PCL polymer ratios. In a mouse model of biofilm-associated orthopedic-implant infection, three different combinations of antibiotic-loaded coatings were highly effective in preventing infection of the bone/joint tissue and implant biofilm formation and were biocompatible with enhanced osseointegration. This nanofiber composite-coating technology could be used to tailor the delivery of combinatorial antimicrobial agents from various metallic implantable devices or prostheses to effectively decrease biofilm-associated infections in patients.

nanofiber | biofilm | infection | antibiotic | delivery

Infection is a devastating complication and a major impediment to the success of implanted medical devices (1), such as orthopedic prostheses (2, 3) and cardiac implantable electrophysiological devices (CIEDs) (4). For prosthetic joint infections (PJIs), the reoperations and extended immobility during treatment result in increased morbidity and mortality (5, 6) and CIED infections can cause life-threatening endocarditis, septic shock, and pulmonary septic emboli (4). Despite advances in aseptic surgical techniques and prophylactic i.v. antibiotics, the incidence of these infections has remained at 1–5% (7, 8), corresponding to ∼25,000 PJIs, 14,000 CIED infections, and 100,000 fracture-fixation device infections per year in the United States (1, 7, 8). Moreover, the number of these infections is rising dramatically along with the increasing clinical demand for these devices (8, 9).

Medical device infections are associated with biofilm formation, which occurs when bacteria adhere to the implants and become embedded in a dense matrix of proteins, polysaccharides, and DNA (10, 11). Biofilms block antibiotic penetration and host immune defenses, resulting in chronic and difficult-to-treat infections (10, 11), and provide a reservoir for antibiotic-resistance genes (12, 13). The treatment of biofilm-associated infections typically involves reoperations to remove or replace the infected implants and prolonged systemic antibiotic therapy (14–16), with inpatient costs averaging ∼$100,000 per patient or an annual national healthcare burden exceeding $4 billion in the United States (7, 17). Current clinical guidelines for systemic antibiotic treatment of medical device infections recommend combinatorial antibiotic therapy because it is more effective than single antibiotics and decreases the potential development of antibiotic resistance while on therapy (14–16).

Because most biofilm-associated infections are caused by invading bacteria in the perioperative period, local antibiotic therapy has been clinically used, including antibiotic-loaded cement, beads, spacers, or powder in orthopedic surgery (18–20) and intraoperative lavage or application of antibiotics in CIED implantation (4, 14). However, most of these approaches are only designed for single antibiotic release, which increases the likelihood of the development of antibiotic resistance while patients are on therapy (21, 22). Therefore, we developed a conformal implant coating capable of local delivery of combinatorial antibiotics with tailored release profiles for each drug to effectively prevent biofilm formation and ensuing infectious complications.

Significance

Biofilm infections are a major complication associated with implantable medical devices and prostheses, which are exceedingly difficult to treat. To date, there has been no effective clinical solution that combines antibacterial efficiency with excellent osseointegration. Here, a nanofiber-based conformal coating capable of controlled and independent local delivery of two or more combinatorial antibiotics was developed to provide optimal antimicrobial activity for the prevention of biofilm-associated infections. In a preclinical animal model of orthopedic-implant infection, this technology demonstrated complete bacterial clearance from the implant and surrounding bone/joint tissue while promoting osseointegration. This tunable nanofiber composite coating could be highly effective in preventing medical device infections in patients.

Author contributions: A.G.A., X.J., J.Z., H.-Q.M., and L.S.M. designed research; A.G.A., X.J., J.Z., A.S.T., W.-S.K., J.M.T., R.J.M., J.H.S., Y.W., C.A.D., A.A.O., and Y.S.C. performed research; A.G.A., X.J., J.Z., W.-S.K., J.M.T., R.J.M., J.H.S., A.A.O., Y.S.C., S.K.J., L.C.J., R.S.S., H.-Q.M., and L.S.M. analyzed data; A.G.A., X.J., J.Z., H.-Q.M., and L.S.M. conceived the technology; and A.G.A., J.Z., J.M.T., S.K.J., L.C.J., R.S.S., H.-Q.M., and L.S.M. wrote the paper.

Conflict of interest statement: The work in this manuscript was included in a provisional patent application submitted on February 8, 2016: "Compositions and Methods for Preparation of Composite Polymer Coatings on Medical Implants, and Their Use for Co-delivery of Multiple Antimicrobial Agents (Johns Hopkins Technology Ventures C13894_P13894-01; WS 111232-00484) - pending." L.S.M. reports grant support from Pfizer and MedImmune and consulting fees from Nantworks and Noveome Biotherapeutics that are outside the submitted work.

This article is a PNAS Direct Submission.

[1]A.G.A. and X.J. contributed equally to this work.

[2]H.-Q.M. and L.S.M. contributed equally to this work.

[3]To whom correspondence may be addressed. Email: lloydmiller@jhmi.edu or hmao@jhu.edu.

This article contains supporting information online at www.pnas.org/lookup/suppl/doi:10.1073/pnas.1613722113/-/DCSupplemental.

Results

Electrospinning to Generate a Nanofiber Composite Coating for Implants. To develop an implant coating capable of combinatorial antibiotic delivery, two antibiotic-loaded polymer solution jets were simultaneously electrospun (23, 24) (i.e., cospinning) onto a medical-grade titanium Kirschner-wire (K-wire) implant (0.5-mm diameter × 9-mm length). Poly(lactic-coglycolic acid) (PLGA) and poly(ϵ-caprolactone) (PCL) were selected because of their proven track records of biocompatibility and bioresorbability in clinical use of various suture and drug delivery devices (25, 26). The coated implants were then heat treated in a continuous airflow of 65–70 °C for 10–15 s to melt the PCL fibers to anneal the composite polymers to produce a conformal coating (Fig. 1*A*). The coating could conform to both smooth and threaded K-wire surfaces (Fig. 1*B*).

This method creates two separate polymer matrices (PLGA fibers and PCL film) that can be used to contain and control the release rates of different antibiotics. The cospinning step allows for sufficient mixing of the two fiber sets before landing onto the K-wire followed by annealing to generate a composite coating with good distribution of the PLGA fibers in PCL film. The coating configuration could be modified by varying the weight ratio of PLGA and PCL deposited to the K-wire. Higher PLGA:PCL ratios resulted in more PLGA nanofibers exposed on the surface and lower PLGA:PCL ratios resulted in the PLGA nanofibers becoming fully embedded in a smooth PCL film (Fig. 1*C*). The composite coating thickness (i.e., the total coating weight) could be modified from ∼10–100 μm (∼0.2–2 mg/K-wire implant) by varying the fiber deposition time and/or the flow rates of the polymer solutions through the syringe pumps (Fig. S1 *A* and *B*).

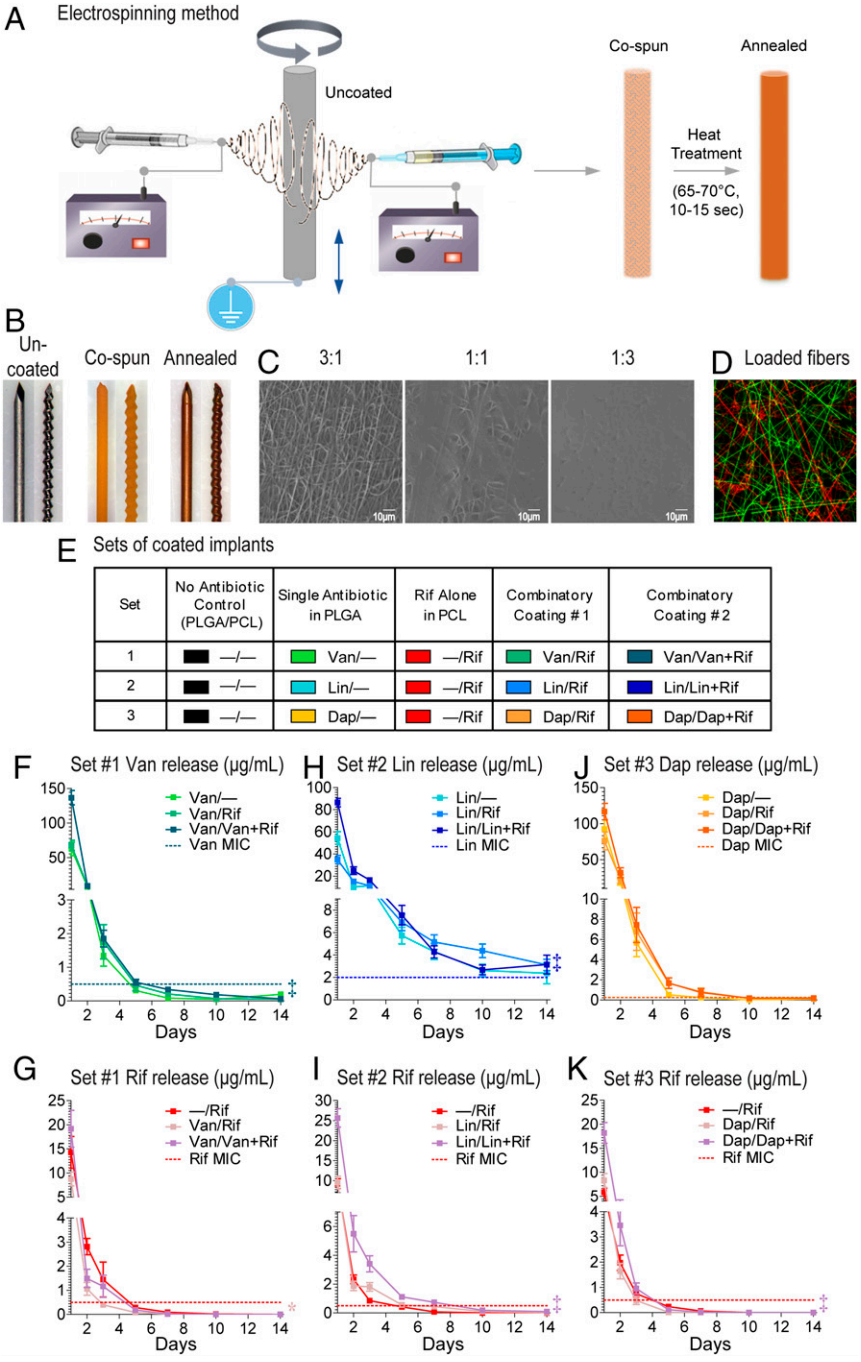

Set	No Antibiotic Control (PLGA/PCL)	Single Antibiotic in PLGA	Rif Alone in PCL	Combinatory Coating #1	Combinatory Coating #2
1	—/—	Van/—	—/Rif	Van/Rif	Van/Van+Rif
2	—/—	Lin/—	—/Rif	Lin/Rif	Lin/Lin+Rif
3	—/—	Dap/—	—/Rif	Dap/Rif	Dap/Dap+Rif

Fig. 1. PLGA/PCL composite implant coating loaded with antibiotics. (*A*) The nanofiber-film coating was prepared by coelectrospinning of antibiotic-loaded PLGA and PCL fibers simultaneously onto the titanium K-wire implants followed by heat treatment to generate a conformal PCL film embedded with PLGA fibers. (*B*) Micrographs of K-wire implants before (*Left*) and after electrospinning (*Middle*) and annealing (*Right*) of the Van/Rif composite coating. (*C*) SEM images of the surface topography of composite coatings prepared with different weight ratios of PLGA:PCL. (*D*) Fluorescent micrograph of a composite coating with two separate sets of PLGA fibers [FITC-loaded (green) and rhodamine-loaded (red)] embedded in PCL film (not visible). (*E*) Antibiotic composite coating configurations for sets 1–3. All implants have the same 1:1 PLGA/PCL coating with different drug combinations. (*F–K*) In vitro antibiotic release profiles (mean micrograms per milliliter ± SEM) measured by placing the coated implants into a new solution of PBS (200 μL) at 37 °C each day for 14 d (n = 10 coated implants per group). Horizontal dotted lines show MIC of Xen36 for each antibiotic: Van (0.5 μg/mL), Lin (2 μg/mL), Dap (0.25 μg/mL), and Rif (0.5 μg/mL). $^{*}P < 0.05$, $^{\dagger}P < 0.01$, $^{\ddagger}P < 0.001$ for combination antibiotic-loaded coatings vs. single antibiotic coatings (two-way ANOVA).

Because the PLGA fibers are separately distributed in the PCL film, it is possible to introduce more than one set of PLGA fibers with different drugs if desired. To demonstrate this possibility, we used two different fluorescent dyes as surrogates for antibiotics and cospun a FITC-loaded PLGA jet, a rhodamine-loaded PLGA jet, and a PCL jet followed by annealing. This process resulted in a composite coating containing two different sets of PLGA fibers with no observed mixing of the dyes (Fig. 1*D*). Because PLGA fibers remained intact, single or combinatorial drugs could be loaded into each distinct polymer fiber jet to tailor the release rate and duration for each drug.

Loading Antibiotics into the Composite Implant Coating. The majority of implanted medical device infections are caused by staphylococcal species, including methicillin-resistant *Staphylococcus aureus* (MRSA) (1, 2, 4). Systemic administration of vancomycin (Van) plus rifampin (Rif) is recommended in clinical practice guidelines to treat these infections (14–16) because combinatorial therapy with Rif has an added therapeutic benefit (27, 28). Newer antistaphylococcal agents such as linezolid (Lin) and daptomycin (Dap) are also used to cover MRSA (29). Although these four antibiotics have different polarities, specific spinning conditions were developed for encapsulating these drugs in either or both compartments, affording flexibility to tailor the release profiles for different drug configurations. Three sets of composite PLGA/PCL coatings loaded with different antibiotic combinations were generated as examples of local combinatorial therapy, with Rif loaded in PCL film and Van or Lin or Dap in PLGA fibers (Fig. 1*E*). To aid in notation, "Van/–" is used to denote a coating configuration where Van is loaded in PLGA fibers and no drug is loaded in PCL film, and "Van/Rif" denotes a coating where Van is loaded in PLGA fibers and Rif is loaded in PCL film. Similar notations are used for other combinations. To increase the loading of Van, Lin, and Dap in their respective coating configuration, another variation of the coating was generated with these antibiotics loaded in both PLGA fibers and the PCL film, i.e., Van/Van + Rif, Lin/Lin + Rif, and Dap/Dap + Rif (Fig. 1*E*). Of note, there is well-known development of Rif resistance by bacteria when Rif is present as a single agent during therapy (14–16). Thus, a desired feature of the antibiotic-loaded composite coatings was to have Rif released faster than the other combinatorial antibiotic to ensure Rif was not present as a single agent during the entire release period.

In Vitro Antibiotic Release Profiles from the Composite Coating. The in vitro release concentrations of the antibiotics from the composite coatings into PBS at 37 °C over 14 d was determined using reverse-phase HPLC detected at specific absorbance wavelengths for each antibiotic. For set 1, the Van release from the all Van composite coatings (Van/–, Van/Rif, and Van/Van + Rif) remained above the minimal inhibitory concentration (MIC) of *S. aureus* strain Xen36 for 3–5 d, whereas the Rif concentrations decreased below the MIC by 3–5 d (Fig. 1 *F* and *G*). For set 2, the Lin release from all of the composite coatings (Lin/–, Lin/Rif, and Lin/Lin + Rif) remained above the MIC for up to 14 d, whereas the Rif concentrations decreased below the MIC between 5 and 10 d (Fig. 1 *H* and *I*). For set 3, the Dap release from the composite coatings (Dap/–, Dap/Rif, and Dap/Dap + Rif) remained above the MIC for 5–10 d, whereas the Rif concentrations decreased below the MIC by 3–5 d (Fig. 1 *J* and *K*). Thus, in all combinatorial coatings, Rif was released faster than Van, Lin, or Dap.

The release profiles of the antibiotics in the different PLGA/PCL coatings were also compared. In set 1, the concentration of Van released from the Van/Van + Rif coating but not from the Van/Rif coating was significantly greater than Van/– coating (Fig. 1*F*). The concentration of Rif released from the Van/Rif coating was slightly but significantly lower than the –/Rif coating (Fig. 1*G*). In set 2, the concentrations of Lin and Rif released from the Lin/Lin + Rif coating but not from the Lin/Rif coating were significantly greater than the Lin/– or –/Rif coatings, respectively (Fig. 1 *H* and *I*). In set 3, there were no statistical differences in the concentrations of released Dap among the Dap coatings (Fig. 1*J*). However, the concentration of Rif released from Dap/Dap + Rif but not Dap/Rif was significantly higher than the –/Rif coating (Fig. 1*K*). It is worth noting that coloading Lin or Dap in PCL film with Rif slowed the release rate of Rif from the composite coating.

Antimicrobial Activity of the Released Antibiotics from Composite Coating. To measure in vitro antimicrobial activity against *S. aureus* [strain Xen36 derived from American Type Culture Collection (ATTC) 49525 (Wright)] (30, 31), zone of inhibition (ZOI) assays were performed using the composite-coated K-wires. The greatest ZOI in each set was observed with Van/Rif and Van/Van + Rif (Fig. 2*A*), Lin/Lin + Rif (Fig. 2*B*), and Dap/Dap + Rif (Fig. 2*C*), which were similar to the ZOI observed with –/Rif. The single antibiotic coatings (i.e., Van/–, Lin/–, and Dap/–) had the smallest ZOIs, which was not due to differences in release from PLGA or PCL because there were no differences in ZOIs for Van, Lin, or Dap when they were loaded into either PLGA or PCL (Fig. S2). Thus, the smaller ZOI for these antibiotics was likely due to inherent properties of these particular antibiotics such as their hydrophobic nature and limited diffusion in agar.

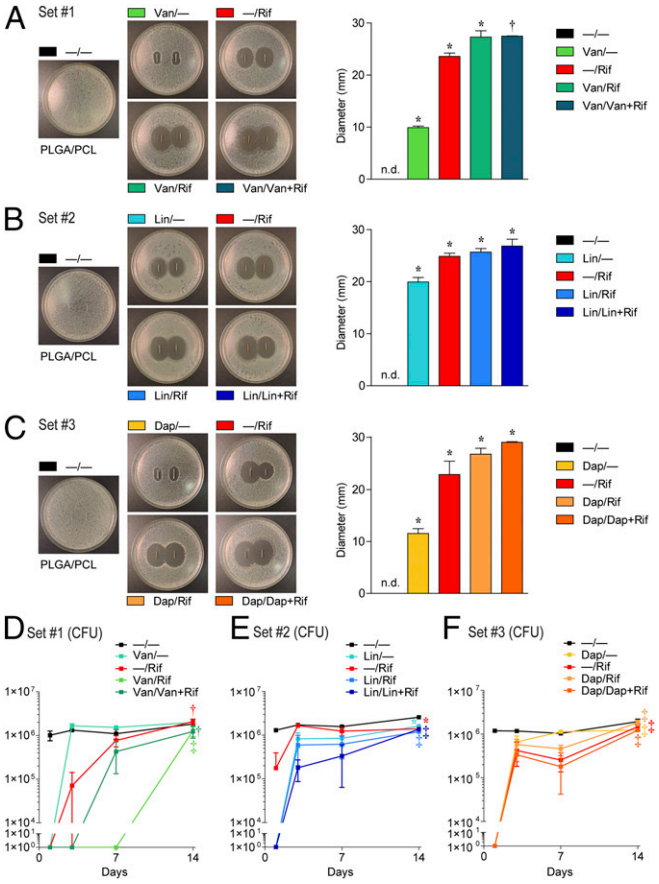

Fig. 2. In vitro antimicrobial activity. Representative ZOI images are shown (*Left*) and ZOI diameter (mean millimeters ± SEM) were measured (*Right*) for set 1 (*A*), 2 (*B*), and 3 (*C*) antibiotic composite coatings (antibiotics loaded into PLGA and PCL are denoted as shown in Fig. 1*E*) after two replicate-coated implants were placed on bacterial culture plates that produced a *S. aureus* lawn. In vitro antimicrobial activity assays were performed by incubating the drug release solutions from the composite-coated implants collected on days 1, 3, 7, and 14, and mean cfu ± SEM (log scale) were enumerated by absorbance (A_{600}) with a cfu standard curve for the coatings in set 1 (*D*), 2 (*E*), and 3 (*F*) ($n = 5$ coated implants per group). $^{*}P < 0.05$, $^{\dagger}P < 0.01$, $^{\ddagger}P < 0.001$ for antibiotic-loaded coatings vs. –/– control coating [two-tailed Student's *t* test (*A*–*C*) or two-way ANOVA (*D*–*F*)].

The in vitro antimicrobial activity was also quantified by mixing the antibiotic release solutions from days 1, 3, 7, and 14 with *S. aureus*-containing broth (1×10^3 cfu/mL) at a 1:1 (vol/vol) ratio and comparing cfu after an 18-h incubation at 37 °C (Fig. 2 *D–F*). Day 1 drug release solutions from the composite coatings of sets 1 and 3 completely inhibited bacterial growth (Fig. 2 *D* and *F*). For set 2, day 1 drug release solutions from the Lin/–, Lin/Rif, and Lin/Lin + Rif composite coatings inhibited bacterial growth (Fig. 2*E*). Some antimicrobial activity was observed with Van/Rif, Van/Van + Rif, Lin/Rif, Lin/Lin + Rif, Dap/Rif, and Dap/Dap + Rif combined coatings through day 7 or longer (Fig. 2 *D–F*), whereas the –/Rif coatings had variable antimicrobial activity on day 1 and minimal activity on subsequent days. Taken together, the best-performing coatings on inhibiting bacterial growth in vitro from each set were Van/Rif, Lin/Lin + Rif, and Dap/Dap + Rif.

Tunability of the Antibiotic-Loaded Composite Coatings. By including the antibiotics into PLGA fibers, PCL film or both PLGA and PCL, this led to optimal release of the antibiotics (Fig. 1 *F–K*) and antimicrobial activity (Fig. 2), suggesting that the antibiotic release from the composite coatings can be tuned. To specifically determine whether the antibiotic release could be tuned by loading the antibiotic in either PLGA or PCL, Van, Lin, Dap, or Rif was loaded into either PLGA or PCL and in vitro release concentrations were determined. Van, Lin, or Rif had significantly slower release from PLGA than from PCL (Fig. 3 *A*, *B*, and *D*), whereas Dap had similar release from PLGA or PCL (Fig. 3*C*).

In addition, to determine whether the antibiotic release could be tuned by varying PLGA:PCL polymer weight ratios, the loading of the best-performing coatings from Fig. 2 (Van/Rif, Lin/Lin + Rif, and Dap/Dap + Rif) were changed from 1:1 to either 3:1 or 1:3 PLGA:PCL and in vitro release concentrations were determined (Fig. 3 *E–J*). In comparing these two configurations, the released concentration of Van, Lin, and Dap was significantly greater and lasted longer in all 3:1 PLGA:PCL coatings than the 1:3 PLGA:PCL coatings (with the exception of day 1 for Lin/Lin + Rif) (Fig. 3 *E*, *G*, and *I*), indicating that the higher PLGA:PCL ratio resulted in a more sustained release of the antibiotics that were loaded into PLGA (i.e., Van, Lin, and Dap). Conversely, the release concentration of Rif from the 1:3 PLGA/PCL coatings were substantially greater and lasted longer than the 3:1 PLGA:PCL coatings (Fig. 3 *F*, *H*, and *J*). In this scenario, Rif was only loaded into PCL and the greater the ratio of PCL, the greater and longer the duration was of Rif release. Taken together, these results indicate that varying the weight ratio of the polymers is another approach that can be used to modulate drug release.

To determine whether these in vitro findings corresponded to differences in in vivo release, a near-infrared (NIR) dye was used as a surrogate for the antibiotics. The NIR dye was loaded into either PLGA (NIR/–) or PCL (–/NIR) at 1:1 ratios onto smooth K-wire implants, which were subsequently surgically placed in a retrograde manner in the right knee joints into the distal femoral intramedullary canal, as in our prior orthopedic implant mouse model (30, 31). To noninvasively monitor the in vivo release of the NIR dye, in vivo fluorescence imaging was performed on the mice to determine the NIR dye signals emitted (Fig. 3 *K* and *L*). The NIR/– coating had significantly higher in vivo fluorescent signals that lasted longer than the –/NIR coating. Thus, the NIR dye was released slower from PLGA than PCL in vivo. These data confirmed that the release rate and duration of the drug surrogate in vivo were dependent on the polymer carrier (PLGA fibers vs. PCL film). Taken together, these in vitro and in vivo data demonstrate that drug release from the PLGA/PCL composite coatings can be tuned by loading the drugs into either PLGA or PCL and by varying the PLGA:PCL weight ratios.

In Vivo Efficacy on Bacterial Burden. An in vivo model of PJI was used to evaluate the in vivo efficacy of the antibiotic-eluting coatings. The same surgical procedures for placing the composite-coated K-wires into the right femoral intramedullary canal were used as in Fig. 3 *K* and *L*, and *S. aureus* (Xen36; 1×10^3 cfu) was pipetted directly onto the protruding implant in the knee joint before closure (30, 31). This model recapitulates many features of human PJI (2, 3), including biofilm formation on the implant, septic arthritis, osteomyelitis, and periprosthetic osteolysis (30, 31). To noninvasively monitor the bacterial burden, in vivo bioluminescence imaging (BLI) was used to detect signals emitted from *S. aureus* strain Xen36, which possesses a stable bioluminescent construct (30, 31). On day 14, cfu from the homogenized bone/joint tissue samples and from the sonicated implants were assayed.

The –/– coating had BLI signals that remained at least a log higher than background through day 14 and correlated with ∼0.5–1×10^6 cfu from the bone/joint tissue and $>1 \times 10^4$ cfu from the implants. In set 1, Van/Rif resulted in decreased BLI signals that approached background levels and had <100 cfu in the bone/joint tissue and no cfu detected from the implants (Fig. 4 *A–C*). Van/Van + Rif had a trend for decreased in vivo BLI signals ($P = 0.067$) and had similar cfu in the bone/joint tissue and implants as Van/Rif. In sets 2 and 3, Lin/Lin + Rif and Dap/Dap + Rif each resulted in BLI signals that approached background levels, and no cfu were detected from the bone/joint tissue or implants (Fig. 4 *D–F* and *G–I*, respectively). In contrast, the coatings containing a single antibiotic Van/–, Lin/–, Dap/–, and –/Rif had variable effects on BLI signals and cfu from the implants, but all had cfu readily detected from the bone/joint tissue. Taken together, the best-performing coatings in vivo in each set were Van/Rif, Lin/Lin + Rif, and Dap/Dap + Rif. As a comparison with the current clinical practice of using only perioperative i.v. antibiotic prophylaxis (15), i.v. Van at the equivalent human exposure dose (32) was evaluated in this model, which resulted in decreased BLI signals but had a minimal reduction in cfu (Fig. S3).

To evaluate whether the best-performing coatings eradicated the infection, ex vivo homogenized bone/joint tissue specimens and ex vivo harvested implants were subsequently cultured in tryptic soy broth (TSB) for 48 h. No bacteria were cultured from the tissue of the Lin/Lin + Rif or Dap/Dap + Rif groups (Fig. 5*A*) or from the implants of the Van/Rif, Lin/Lin + Rif, or Dap/Dap + Rif groups (Fig. 5*B*). Finally, antibiotic blood levels at 8, 24, and 48 h and 7 d after implantation were also measured for the best-performing coatings in vivo (Van/Rif, Lin/Lin + Rif, and Dap/Dap + Rif). The levels of all antibiotics were below the level of detection (200 ng/mL for Van, 134 ng/mL for Rif, and 70 ng/mL for Lin and Dap in serum samples at a signal-to-noise ratio of 2), indicating that systemic exposure to the locally delivered antibiotics was negligible.

In Vivo Efficacy on Biofilm Formation. On day 14, the ex vivo harvested implants were processed for SEM analysis to evaluate biofilm formation (Fig. 5*C*). The –/– coatings had biofilm formation with coccoid bacteria characteristic of *S. aureus* within an extracellular biofilm matrix (33). No biofilms were observed on implants coated with Van/Rif, Lin/Lin + Rif, or Dap/Dap + Rif, demonstrating the ability of the antibiotic-loaded composite coatings to prevent biofilm formation.

In Vivo Efficacy on Osteolysis and Osseointegration. To determine whether the antibiotic-eluting composite coatings could prevent reactive bone expansion associated with the periprosthetic osteolysis that progresses in this orthopedic implant infection model (30), high-resolution X-rays were obtained on day 14 and femur width and area were measured by image analysis (Fig. 6 *A–C*). The –/– coatings had significantly increased femur width and area compared with uninfected controls. The best-performing coatings, Van/Rif, Lin/Lin + Rif, and Dap/Dap + Rif, had smaller femur width and area than the –/– control coatings and comparable femur width and area to –/– coatings in uninfected (sterile) mice (Fig. 6 *A–C*). For the other antibiotic-loaded composite coatings in sets 1–3, the femur widths and areas were significantly decreased compared with the –/– control coating (with the exception of Van/– and Dap/–) and were smaller or not significantly different than –/– coatings in uninfected (sterile) mice (with the exception of Van/– and Lin/Rif, and Dap/–) (Fig. S4). Thus, almost all of the antibiotic-loaded coatings had some degree of efficacy in preventing infection-induced reactive bone changes.

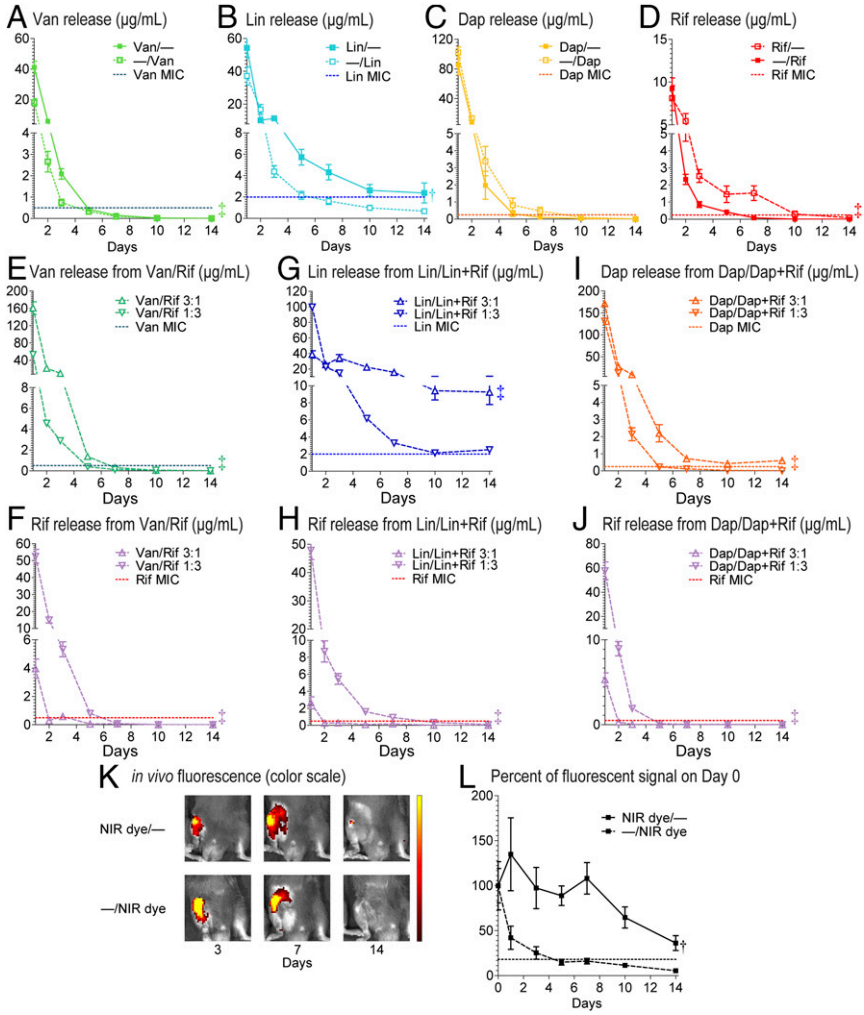

Fig. 3. Tunability of the composite coatings. In vitro antibiotic release profiles (mean micrograms per milliliter ± SEM) of the antibiotic composite coatings (antibiotics loaded into PLGA and PCL are denoted as shown in Fig. 1*E*) were measured after varying polymer loading (*A*–*D*) and polymer weight ratios (*E*–*J*) during electrospinning by placing the coated implants into a new solution of PBS (200 μL) at 37 °C each day for 14 d ($n = 10$ coated implants per group). Horizontal dotted lines show MIC of Xen36 for each antibiotic: Van (0.5 μg/mL), Lin (2 μg/mL), Dap (0.25 μg/mL), and Rif (0.5 μg/mL). $^{*}P < 0.05$, $^{\dagger}P < 0.01$, $^{\ddagger}P < 0.001$ for combination antibiotic-loaded coatings vs. single antibiotic coatings (two-way ANOVA) on data from all days (1–14), except *D* and *G*, which included data from days 2–14. In vivo release of a NIR fluorescent dye (VivoTag-S 680) loaded into PLGA (NIR dye/–) or PCL (NIR dye/–) was examined in an orthopedic implant mouse model. (*K*) Representative in vivo fluorescence images. (*L*) Mean percentage of total radiant efficiency ([p/s]/[μW/cm^2]) signal on day 0 ± SEM $^{\dagger}P < 0.01$ for NIR dye/– vs. –/NIR dye (two-way ANOVA).

In addition, μCT analysis demonstrated that femur density was increased in the best-performing coating groups compared with the –/– controls (Fig. 6 *D* and *E*). However, the femur density in each of the best performing coating groups was significantly less than the density of –/– coatings in uninfected (sterile) mice, indicating that even though the infection was cleared, the bone density changes induced by the infection did not completely resolve by the end of the experiment on day 14.

To determine whether the composite coatings were biocompatible by facilitating osseointegration, the coatings were evaluated on threaded K-wire implants using histomorphometry and biomechanical pullout testing (Fig. 7). By histomorphometry, the Van/Rif, Lin/Lin + Rif, and Dap/Dap + Rif coatings all had increased new bone formation at the implant/coating interface compared with the –/– coatings in infected mice (Fig. 7 *A* and *B*). Mechanical pullout testing revealed that the –/– coatings in infected implants had a threefold lower pullout force than uninfected control mice (Fig. 7*C*). Of the best-performing coatings, Lin/Lin + Rif and Dap/Dap + Rif coatings, but not the Van/Rif coating, yielded pullout forces significantly greater than –/– coatings in infected mice. None of the antibiotic coatings had pullout forces that were statistically different from –/– coatings in uninfected (sterile) mice.

Durability and Stability of Antibiotic-Loaded Coated Implants. To evaluate durability of these implant coatings, the ability of the coatings to withstand surgical implantation was evaluated by comparing coatings without (cospun) and with (annealed) heat treatment. Without heat treatment, the coating peeled back during insertion into the femoral intramedullary canal (Fig. 8*A*). In contrast, with heat treatment, the coated implant could be inserted and immediately removed from the femoral intramedullary canal without damage to the coating (Fig. 8*B*), indicating that the heat-treated coatings could withstand typical surgical handling.

To evaluate the long-term stability, in vitro release of the antibiotics was performed on newly coated implants loaded with single antibiotics and on the same implants stored after 6 wk at −20 °C or room temperature. After storage at −20 °C or room temperature for 6 wk, Van-, Lin-, and Dap-loaded coatings had release rates that did not significantly differ from newly coated implants (Fig. 8 *C*–*E*). The Rif-loaded coating also maintained nearly the same release profile when stored at −20 °C for 6 wk (Fig. 8*F*). However, Rif release concentrations were significantly decreased when

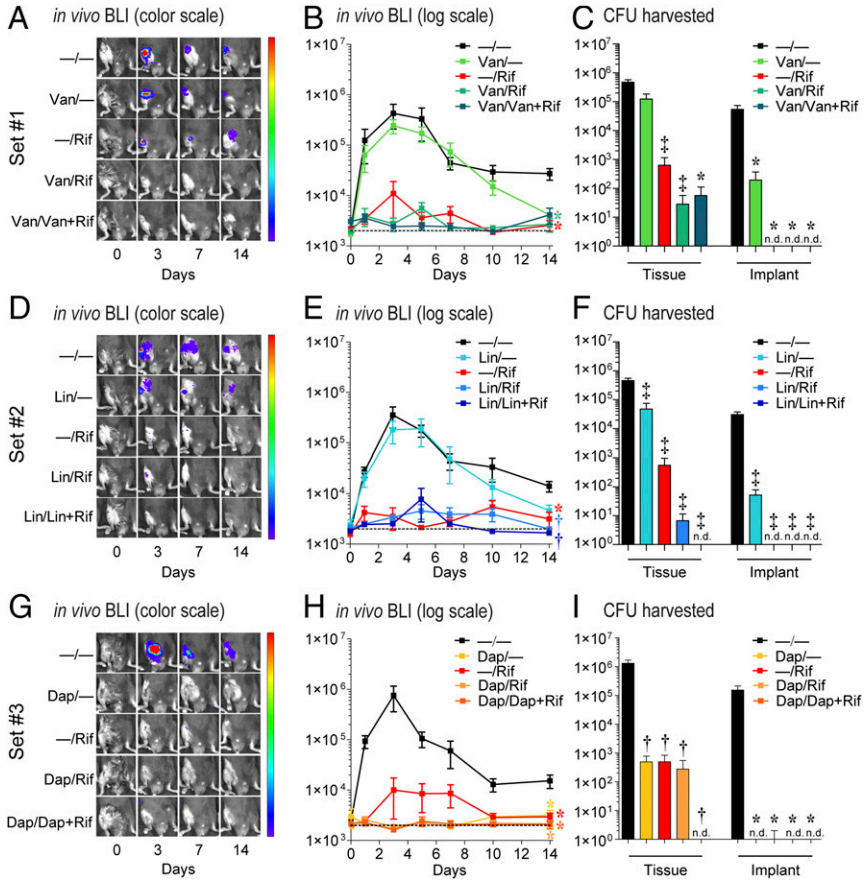

Fig. 4. In vivo efficacy on bacterial burden. Using a mouse PJI model, the efficacy of the sets 1–3 antibiotic composite coatings (antibiotics loaded into PLGA and PCL are denoted as shown in Fig. 1*E*) was evaluated using in vivo BLI (n = 15–20 mice per group) and ex vivo cfu counting on harvested bone/joint tissue and implants on day 14 (n = 10–15 mice per group). (*A*, *D*, and *G*) Representative in vivo BLI images. (*B*, *E*, and *H*) Mean maximum flux (photons per second) ± SEM (*C*, *F*, and *I*) mean cfu ± SEM $^{*}P < 0.05$, $^{\dagger}P < 0.01$, $^{\ddagger}P < 0.001$ for antibiotic-loaded coatings vs. –/– control coating [two-way ANOVA (*B*, *E*, and *H*) or two-tailed Student's t test (*C*, *F*, and *I*)]. n.d., not detected. Data represent two to three independent experiments.

stored at room temperature for 6 wk compared with newly coated implants (Fig. 8*F*). In addition, in vitro antimicrobial activity after storage was evaluated using ZOI assays as in Fig. 3 for the above groups as well for implants stored at −20 °C for 8 mo, and the ZOIs were not significantly decreased for any of the stored implants compared with newly coated implants (Fig. 8*G*). Taken together, storage at room temperature did not impact Van, Lin, or Dap release but did result in slightly decreased Rif release, and all storage conditions (−20 °C or room temperature for 6 wk or −20 °C for 8 mo) did not significantly impact the in vitro antimicrobial activity compared with newly coated implants.

Discussion

To prevent biofilm-associated infections during the perioperative period, a nanofiber composite implant coating capable of local and sustained delivery of combinatorial antibiotics was developed. This coating used electrospinning techniques (34, 35), which permitted the cospinning of two or more separate polymer fibers with different compositions and release kinetics that were loaded with two (or potentially more) antibiotics to provide a unique approach to control and optimize local drug delivery from the implant surface. The successful generation of this conformal coating was facilitated by the low annealing temperature, which was high enough to melt the PCL fibers but low enough not to inflict any potential effects on antibiotic activity.

This method offers a versatile composite coating on the implant surface due to the wide range of PLGA polymeric compositions (varying fractions of L-lactide, D,L-lactide, and glycolide) with different molecular weights and the various possible coating parameters (fiber-to-film weight ratio, fiber diameters, coating thickness, drug–polymer pairing, and drug-loading level). As a proof of principle, here we chose only PLGA (75/25, 87 kDa) and PCL (45 kDa) polymers for this study to encapsulate three sets of dual drug combinations: Van + Rif (set 1), commonly used as a systemic antibiotic combination to treat biofilm-associated infections (14–16), Lin + Rif (set 2), and Dap + Rif (set 3), because Lin and Dap also have excellent coverage against MRSA and are second-line antibiotics to treat PJI (29). Additional sets of PLGA fibers can be included in the PCL film through either sequential or simultaneous electrospinning/annealing, so more complex antibiotic-loading configurations can be constructed.

An important characteristic of this PLGA/PCL composite implant coating is that the release of the antibiotic could be tuned by loading the drug into PLGA or PCL, which generally resulted in different release rates in these two polymer compartments. The drug release could also be tuned by varying the polymer weight ratio in the composite coating. The reason for the slower antibiotic release from PLGA and faster antibiotic release from PCL remains to be fully examined, but could be due to the higher solubility of these drugs and thus faster diffusion in PCL film of the composite coatings. Of note, the tunable antibiotic delivery was taken advantage of in this study by loading Rif only into PCL for faster release and shorter duration than the second combinatorial antibiotics to ensure Rif was never present as a single agent to prevent the known rapid development of Rif-resistance during therapy (14–16). Van, Lin, or Dap was loaded in PLGA for more sustained release.

It should be mentioned that coloading two different drugs in the composite coating might cause interference in their release kinetics. For example, even though the durations of Rif release were similar for combinatorial coatings, antibiotic release was moderately impacted by the presence of the second antibiotics in some of the configurations. For example, the released concentrations of Rif were increased when Lin and Dap were also coloaded into PCL film and the released concentrations of Rif were decreased in the Van/Rif coating (Fig. 1 *G*, *I*, and *K*). The reasons for these differences are not entirely clear, but they underscore the importance of performing in vitro release and antimicrobial studies particularly

A Percent of mice with infected tissue

Group	% Infected	*p*-value
–/–	100	-
Van/Rif	40	n.s.
Lin/Lin+Rif	0	< 0.01
Dap/Dap+Rif	0	< 0.01

B Percent of mice with infected implants

Group	% Infected	*p*-value
–/–	80	-
Van/Rif	0	< 0.05
Lin/Lin+Rif	0	< 0.05
Dap/Dap+Rif	0	< 0.05

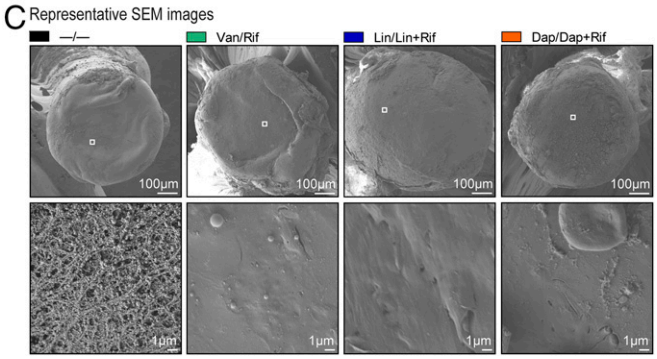

Fig. 5. In vivo efficacy on eradication of infection and biofilm formation. The percent of mice with infected bone/joint tissue (*A*) or ex vivo implants (*B*) harvested on day 14 after surgical placement of the antibiotic composite coatings (antibiotics loaded into PLGA and PCL are denoted as shown in Fig. 1*E*) was determined by evaluating the presence/absence of cfu after 48 h of broth culture ($n = 5$ mice per group). $^{*}P < 0.05$, $^{\dagger}P < 0.01$, $^{\ddagger}P < 0.001$ for antibiotic-loaded coatings vs. –/– control coating (one-tailed Fischer's exact test). (*C*) Biofilm formation was assessed by SEM on ex vivo implants harvested on day 7 and representative low (*Top*) and high (*Bottom*) magnification of the boxed areas in the *Top* are shown ($n = 3$ mice per group).

for combination antibiotic-loaded composite coatings. The release results shown here collectively demonstrated that there is a wide parameter space for tailoring the release profiles for different antibiotic combinations. These analyses can help with further optimization for designing composite coating on devices with different geometries and sizes.

All three sets of composite coatings showed superior antimicrobial efficacy when combinatorial antibiotics were used. The best-performing coatings in each set were Van/Rif, Lin/Lin + Rif, and Dap/Dap + Rif in the in vitro release and antimicrobial assays. In an in vivo mouse model of a *S. aureus* PJI (30, 31), Lin/Lin + Rif and Dap/Dap + Rif completely prevented bacterial infection. All of the combinatorial antibiotic implant coatings outperformed i.v. Van prophylaxis (32), which had only a minimal effect on reducing cfu. In addition, Van/Rif, Lin/Lin + Rif, and Dap/Dap + Rif inhibited biofilm formation on the implant and prevented infection-induced bone changes. Of note, Lin/Lin + Rif and Dap/Dap + Rif coatings were more effective at preventing infection, reducing infection-associated bone changes, and promoting bone-implant contact and osseointegration than the Van/Rif coating. The particular efficacy of Lin + Rif or Dap + Rif combinations might be due to added antibiofilm activity (32, 36–38), warranting further investigation. Van acts by inhibiting cell wall synthesis, so the inferior efficacy of Van/Rif (and Van/Van + Rif) could be due to reduced Van activity against bacteria in biofilms that have increased cell wall thickness (39). It should be mentioned that although we used only a single *S. aureus* strain for this work, we previously found that Xen36 resulted in a similar infectious course in our mouse model of PJI as a community-acquired MRSA isolate (USA300 LAC::*lux*) (32) as well as a human osteomyelitis isolate UAMS1 (Xen40) and it also expresses the *S. aureus*-binding adhesion (*cna*) (31), which is important in the pathogenesis of osteomyelitis, suggesting that the antimicrobial activity of these coatings on Xen36 could be relevant to other clinical *S. aureus* isolates.

An important consideration for the clinical use of an antibiotic-eluting implant coating is biocompatibility, which influences the performance, stability, and longevity of the implant (40). PLGA and PCL have long been known to be biocompatible and bioresorbable and can even promote cell and tissue adhesion (41, 42). All of the best-performing coatings promoted bone-implant contact, and the degree of osseointegration with Lin/Lin + Rif and Dap/Dap + Rif coatings was the same as observed in the absence of any bacterial infection.

Beyond the particular antibiotic combinations evaluated, this PLGA/PCL composite coating could be used for the tunable delivery of various combinations of these and other antibiotics, representing a

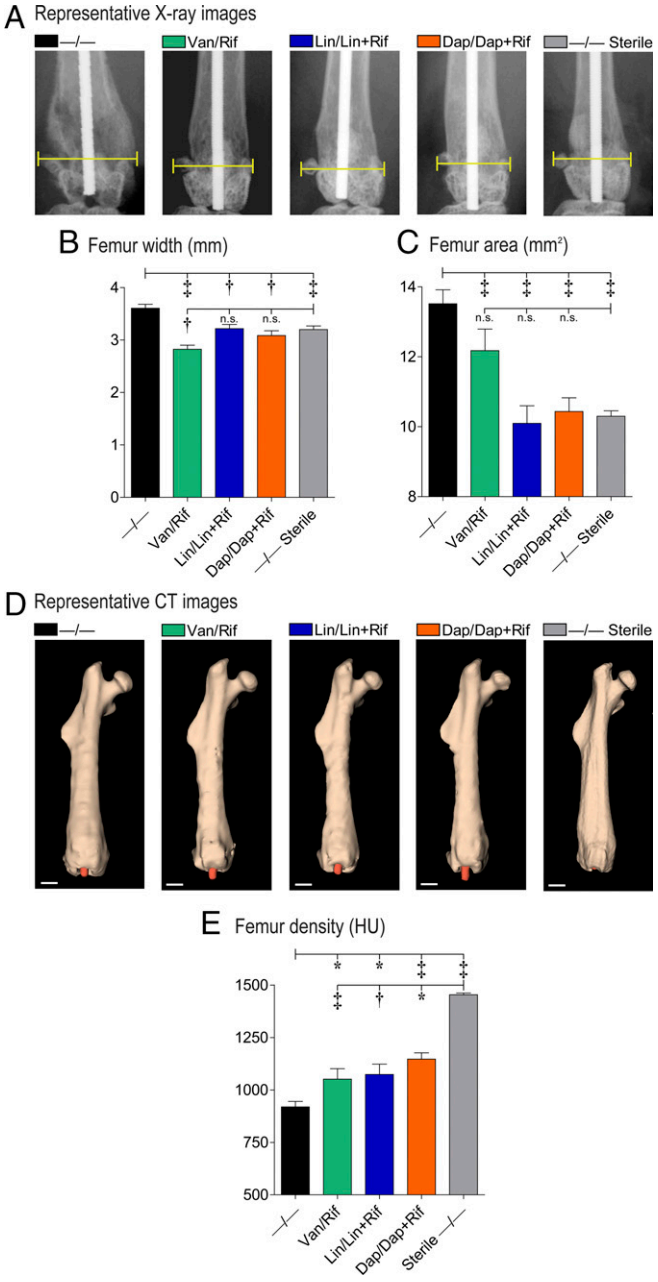

Fig. 6. In vivo analysis of bone changes around the composite implant. Using an in vivo PJI model, high-resolution AP X-rays and μCT images of the distal femurs were obtained on day 14 after placement of the antibiotic composite coatings (antibiotics loaded into PLGA and PCL are denoted as shown in Fig. 1*E*) ($n = 5$ mice per group). (*A*) Representative X-ray images. (*B*) Mean femur width (millimeters ± SEM). (*C*) Mean femur area (square millimeters ± SEM). (*D*) Representative μCT images. (Scale bars, 1 mm.) (*E*) Mean femur density (HU ± SEM). $^{*}P < 0.05$, $^{\dagger}P < 0.01$, $^{\ddagger}P < 0.001$ for antibiotic-loaded coatings vs. –/– control coating (one-tailed unpaired Student's *t* test).

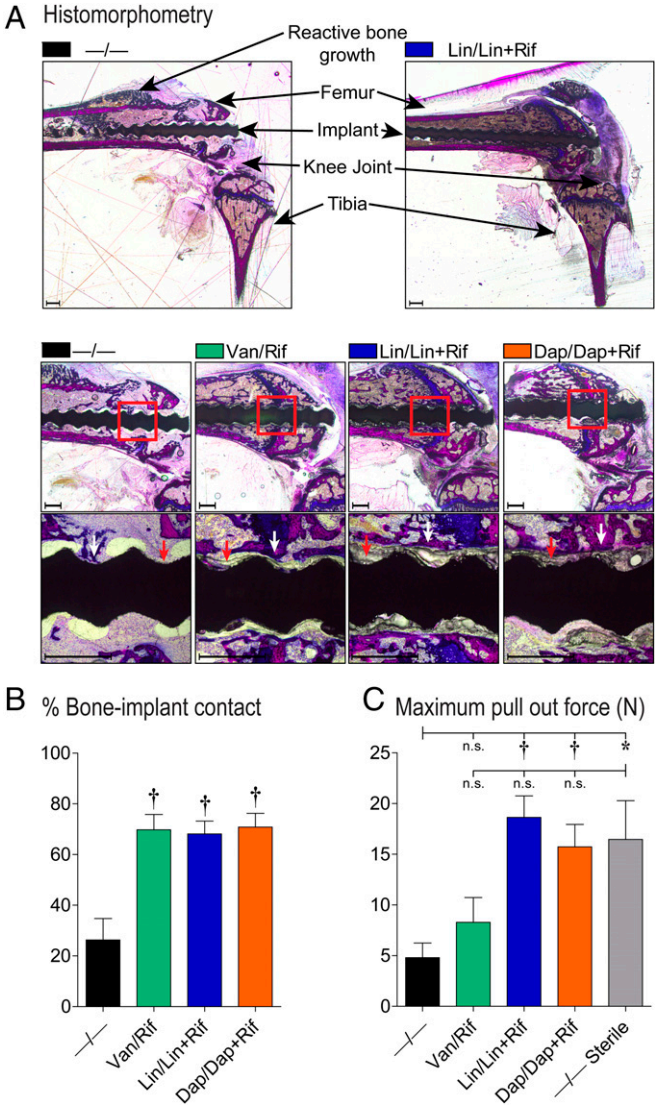

Fig. 7. In vivo analysis on osseointegration. Using an in vivo PJI model, the efficacy of the antibiotic composite coatings (antibiotics loaded into PLGA and PCL are denoted as shown in Fig. 1*E*) in promoting osseointegration was evaluated (n = 5 mice per group). (*A*) Representative histomorphometry sections of undecalcified bone/implant specimens stained with Sanderson's rapid bone stain with an acid fuchsin counterstain. (Scale bar, 500 μm.) (*B*) Mean percentage bone-implant contact ± SEM (red arrows denote examples of coating on the implants and white arrows denote examples of bone contact to the coated implants) (n = 3 mice per group). (*C*) Biomechanical pullout testing was used to measure the force (mean N ± SEM) required to pull the threaded implants from the femurs (n = 5 mice per group). $^{*}P < 0.05$, $^{\dagger}P < 0.01$, $^{\ddagger}P < 0.001$ for antibiotic-loaded coatings vs. –/– control coating or –/– coating in uninfected (sterile) mice (two-tailed unpaired Student's t test).

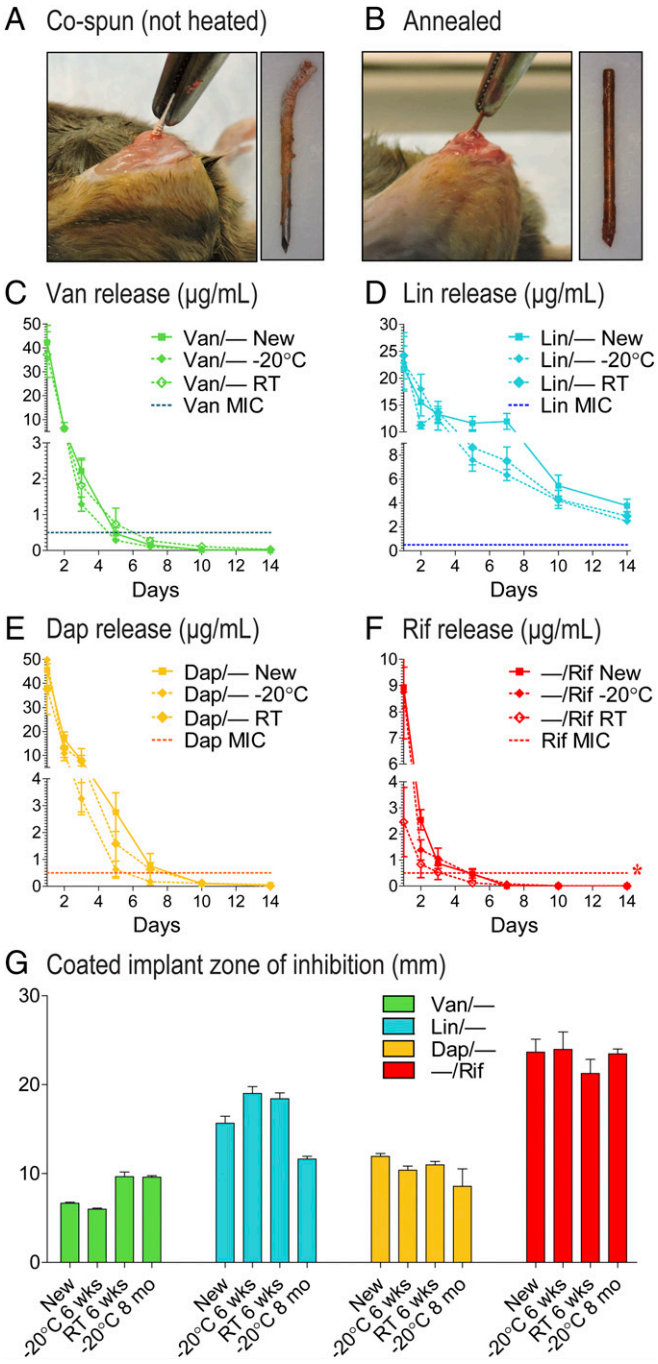

Fig. 8. Durability and stability. Representative photographs of implants that were coated without (*A*) or with (*B*) heat treatment were surgically implanted and immediately removed. (*C*–*F*) In vitro antibiotic release profiles (mean micrograms per milliliter ± SEM) of antibiotic composite coatings (antibiotics loaded into PLGA and PCL are denoted as shown in Fig. 1*E*) that were newly coated (new) or stored at −20 °C or room temperature (RT) for 6 wk were measured by placing the coated implants into a new solution of PBS (200 μL) at 37 °C each day for 14 d (n = 10 coated implants per group). Horizontal dotted lines show MIC of Xen36 for each antibiotic: Van (0.5 μg/mL), Lin (2 μg/mL), Dap (0.25 μg/mL), and Rif (0.5 μg/mL). (*G*) ZOI diameter (mean millimeters ± SEM) was measured for implants that were newly coated (new) or stored at −20 °C for 6 wk, RT for 6 wk, or −20 °C for 8 mo after two replicate-coated implants were placed on bacterial culture plates that produced a *S. aureus* lawn. $^{*}P < 0.05$, $^{\dagger}P < 0.01$, $^{\ddagger}P < 0.001$ for stored vs. newly coated antibiotic-loaded coatings [two-way ANOVA (*C*–*F*) or two-tailed unpaired Student's t test (*G*)].

significant advance over existing antibiotic-releasing approaches used clinically. Currently used antibiotic-loaded cement, beads, and spacers or powder do not confer tunable release of multiple antibiotics (18–20). This may compromise the treatment efficiency and it increases the likelihood of the development of antibiotic resistance while patients are on therapy (21, 22), which has been seen in as high as 50% of patients with PJI treated with gentamicin or tobramycin spacers (43). A recently approved dual antibiotic release mesh envelope impregnated with minocycline and rifampin has proven effective in preventing CIED infection in patients (44, 45). However, although this approach uses two antibiotics, it is not feasible for implants that require a secure fit

within musculoskeletal or organ tissue. Furthermore, the composite coating described here could be used to load agents other than antibiotics such as various antimicrobial materials in early stage development to prevent biofilm-associated infections (e.g., hydrophilic or zwitterionic polymers, surfactants, nanostructured biomaterials, nitric oxide, antimicrobial peptides, or biofilm dispersing agents) (46, 47).

This improved composite, conformal coating with tunable antibiotic codelivery could have broad utility as it can conform to complex metallic surfaces and thus be used to prevent infection of many clinical prostheses, devices, or implants. The polymers and antibiotics used to generate this implant coating have long track records of clinical use, which could facilitate the rapid translation of this technology to meet the urgent need to decrease biofilm-associated infections in patients.

Methods

Electrospinning to Generate a Composite Implant Coating. PLGA (75:25, MW 66,000–107,000; Sigma) and PCL (MW 45,000; Sigma) solutions, each loaded with different antibiotic(s) dissolved in the solution, were electrospun onto medical-grade smooth or threaded titanium K-wires (0.5-mm diameter × 9-mm length; Modern Grinding) using a cospinning process in which two separate, opposite injection streams were sprayed simultaneously onto the implant. Polymer solutions were loaded into separate 1-mL syringes fitted with a 27-gauge blunt-end needle. High-voltage power supplies were connected to the needles through alligator clips and a voltage differential of 6–7 kV was applied between the needle and the K-wire. Two syringe pumps were used to feed the polymer solutions through the needle tips at a flow rate of 0.5 mL/h. The nanofibers were collected simultaneously and directly onto the grounded K-wire at a distance of 10 cm from both needle tips, over a collection time of 1 min per K-wire. The coated K-wire were then heat treated in a continuous airflow at 65–70 °C for 10–15 s to obtain a conformal coating. The PLGA solution [10.0 (wt/wt%) in hexafluoro-2-propanol (HFIP); Sigma] was loaded with either 1% (wt/wt%) Lin (Sigma), Van (Sigma), or Dap (EMD Millipore)]. The PCL solution [10.0 (wt/wt%) in dichloromethane/2-propanol; 4:1 (wt/wt); Sigma] was loaded with 1% (wt/wt%) Rif (Sigma) and/or Van, Lin, or Dap. Van and Dap were first dissolved in 20 μL of DMSO before dispersion in PCL or PLGA solutions. A composite coating on a K-wire without antibiotics was used as the negative control group (–/–). To test the effect of polymer weight ratio in the composite coating on antibiotic release, three specific PLGA/PCL composite configurations loaded with Van/Rif, Lin/Lin + Rif, and Dap/Dap + Rif, respectively, were prepared by electrospinning the same set of polymer solutions (with the same drug and polymer concentrations as described above), but the PLGA:PCL polymer weight ratio was changed from 1:1 to either 3:1 or 1:3 by adjusting the flow rates from the syringe pumps during electrospinning to 0.75 mL/h PLGA and 0.25 mL/h PCL for 3:1 PLGA/PCL coating and 0.25 mL/h PLGA and 0.75 mL/h PCL for 1:3 PLGA/PCL coating. As a result, Van loading varied with the polymer weight ratio, whereas Lin and Dap loadings were the same between these two coatings and with the 1:1 PLGA:PCL weight ratio of the coatings.

In Vitro Release Profiles of Antibiotics from the Composite Coatings. Drug release studies were conducted using coated pins created with the same loading parameters as detailed above. Release kinetics of antibiotics from the composite coating were characterized by placing coated pins in 200 μL of PBS (pH 7.4) at 37 °C. Release media was changed daily over a period of 2 wk and stored at −20 °C until analysis. Drug concentrations in release media were measured on days 1, 2, 3, 5, 7, 10, and 14 using a Waters Alliance 2690 HPLC system (Waters Corporation) equipped with an Accucore RP-MS C18 column (100 mm × 2.1 mm; Thermo Fisher Scientific) and a Waters 2996 PDA detector. The elution was carried out with a mobile phase of water and acetonitrile both mixed with 0.1% TFA at a flow rate of 1 mL/min at ambient temperature using a linear gradient elution program of 85% water to 60% acetonitrile in 15 min. Concentrations of the drugs were quantified using wavelengths for Van (280 nm), Lin (254 nm), Dap (224 nm), and Rif (263 nm).

***S. aureus* Bioluminescent Strain.** *S. aureus* strain Xen36 (PerkinElmer) previously derived from the clinical bacteremia isolate ATCC 49525 (Wright) was used in all experiments (48). Xen36 possesses a bioluminescent construct that is integrated on a stable plasmid that is maintained in all progeny without selection (48). Xen36 was prepared for inoculation as previously described (30, 31).

In Vitro Zone of Inhibition Assay. Tryptic soy agar (TSA) bacterial plates were inoculated with *S. aureus* to yield a bacterial lawn after overnight culture. Before culturing the plates, two titanium K-wires each loaded with the same combination of antibiotics from each set were placed in two separate areas on the plate. After culturing at 37 °C for 24 h, the ZOI (diameter/millimeters) of bacterial growth were measured.

In Vitro Antimicrobial Activity Assay. Midlogarithmic-phase Xen36 bacteria were prepared as above and diluted to 1×10^3 cfu/mL in cation-adjusted Mueller Hinton II broth (CAMHB) (Becton Dickinson) pH 7.3. Bacteria were then cultured 1:1 with drug release solutions collected on days 1, 3, 7, and 14 at 37 °C for 18 h and cfu were enumerated by absorbance (A_{600}) and a standard curve of cfu.

Mice. Ten-week-old male C57BL/6 mice were obtained from The Jackson Laboratory. All animal experiments were approved by the Johns Hopkins University Animal Care and Use Committee (ACUC Protocol no. MO15M421).

Mouse Surgical Procedures for K-Wire Implantation. An established orthopedic implant mouse model was used as previously described (30, 31). Briefly, a medial parapatellar arthrotomy on the right knee was performed and a femoral intramedullary canal was manually reamed with a 25-gauge needle followed by a 23-gauge needle. The coated K-wires were then surgically placed in a retrograde fashion with 1 mm protruding into the joint space. For experiments using the PJI model, an inoculum of Xen36 (1×10^3 cfu in 2 μl PBS) was pipetted on top of the protruding implant before closure. Sustained-release buprenorphine (2.5 mg/kg) (ZooPharm) was administered s.c. at the time of surgery.

In Vivo BLI. Noninvasive and longitudinal measurements of the bacterial burden were performed using in vivo BLI using the Lumina III IVIS (PerkinElmer). Data were quantified as maximum radiance (photons/second/centimeter squared/steradian) within a circular region of interest (1×10^3 pixels) using Living Image software (PerkinElmer) as previously described (30, 31).

Quantification of Bacteria Counts (cfu) from Bone/Joint Tissue and Implants. Mice were killed on day 14 and bacteria from the periimplant bone/joint tissue and implants were isolated and enumerated as previously described (30, 31). In some experiments, bone/tissue homogenates and implants were cultured in TSB at 37 °C for 48 h in a shaking incubator at 240 rpm and plated on TSA plates to determine whether the infection had been eradicated.

Scanning Electron Microscopy. K-wires were removed from the femur at 7 d after the procedure and fixed in buffered 4% formaldehyde/2.5% glutaraldehyde solution for 16 h. All samples were postfixed in 1% osmium tetraoxide in PBS for 2 h, followed by subsequent dehydration in a graded ethanol series. Samples were then placed into transitional series of graded ethanol:hexamethyldisilazane (HMDS) mixtures (2:1, 1:1, and 1:2; each for 30 min), and finally to pure HMDS (twice, 30 min each). Specimens were air dried under a chemical hood before being sputter coated with a gold–palladium alloy and imaged under a field emission scanning electron microscope (SEM) (JSM-6700F FE-SEM; JEOL).

High-Resolution X-Ray Imaging. Mice were killed on postoperative day 14, and the knee joints were visualized with anteroposterior (AP) radiographs using the Faxitron MX-20 Specimen Radiography System (Faxitron Bioptics). AP femur width (width in millimeters) was measured as the maximum femoral width in the AP radiograph and the distal cortical area (area in millimeters squared) was measured as the femoral cortical area distal to the midpoint of the K-wire using the ImageJ analysis software program (imagej.nih.gov/ij/) as previously described (30). X-rays were obtained and analyzed by an experienced orthopedic surgeon who was blinded to the treatment groups.

μCT Imaging. Live mice were imaged on postoperative day 14 within a sealed biocontainment device (Minerve) as previously described (49). A standard small animal anesthesia machine was used to deliver an isoflurane (Henry Schein) and oxygen mixture during transport and imaging. Each animal was imaged using the NanoSPECT/CT small animal imager (Bioscan) with the following settings: X-ray tube potential 55 kVp, intensity 0.143 mA, and integration time of 1,000 ms. Images were reconstructed and visualized using VivoQuant 2.50 (inviCRO). Briefly, the femur was aligned with the vertical axis and the femoral length was measured between the center of the femoral head and the center of the femoral notch. The distal 25% of the femur was analyzed as most of the bone changes were limited to this location. To compensate for the limitation of the image artifacts from the titanium K-wire, a semiautomated approach of connected thresholding was used, based on voxel density measured as Hounsfield units (HU). The voxels within a range of 5,000–50,000 HU or 700–4,999 HU were selected for the titanium K-wire implant or bone region of interest (ROI), respectively. Data

were analyzed by two independent personnel who were blinded to the treatments. Three dimensional images were obtained from contoured 2D images and density measurements were reported as HU.

Statistical Analysis. Data for single comparisons were compared using a Student's *t* test or Fischer's exact test (one or two tailed) and data for multiple comparisons were compared using a two-way ANOVA, as specifically indicated in the figure legends. All data are expressed as mean ± SEM. Values of $P < 0.05$ were considered statistically significant.

SI Methods describes the following methods: in vivo fluorescence imaging, vancomycin i.v. prophylaxis, serum drug level analysis, biomechanical pullout testing, and histomorphometry.

ACKNOWLEDGMENTS. This work was funded in part by a Nexus Award (to H.-Q.M. and L.S.M.), a program supported by the Johns Hopkins Institute for Clinical and Translational Research (ICTR) funded in part by Grant UL1TR001079 from the National Center for Advancing Translational Sciences (NCATS) of the NIH and NIH Roadmap for Medical Research.

1. Darouiche RO (2004) Treatment of infections associated with surgical implants. *N Engl J Med* 350(14):1422–1429.
2. Del Pozo JL, Patel R (2009) Clinical practice. Infection associated with prosthetic joints. *N Engl J Med* 361(8):787–794.
3. Zimmerli W, Trampuz A, Ochsner PE (2004) Prosthetic-joint infections. *N Engl J Med* 351(16):1645–1654.
4. Baddour LM, Cha YM, Wilson WR (2012) Clinical practice. Infections of cardiovascular implantable electronic devices. *N Engl J Med* 367(9):842–849.
5. Cram P, et al. (2012) Total knee arthroplasty volume, utilization, and outcomes among Medicare beneficiaries, 1991-2010. *JAMA* 308(12):1227–1236.
6. Wolf BR, Lu X, Li Y, Callaghan JJ, Cram P (2012) Adverse outcomes in hip arthroplasty: Long-term trends. *J Bone Joint Surg Am* 94(14):e103.
7. Kurtz SM, Lau E, Watson H, Schmier JK, Parvizi J (2012) Economic burden of periprosthetic joint infection in the United States. *J Arthroplasty* 27(8, Suppl):61–5.e1.
8. Voigt A, Shalaby A, Saba S (2010) Continued rise in rates of cardiovascular implantable electronic device infections in the United States: Temporal trends and causative insights. *Pacing Clin Electrophysiol* 33(4):414–419.
9. Kurtz S, Ong K, Lau E, Mowat F, Halpern M (2007) Projections of primary and revision hip and knee arthroplasty in the United States from 2005 to 2030. *J Bone Joint Surg Am* 89(4):780–785.
10. Costerton JW, Stewart PS, Greenberg EP (1999) Bacterial biofilms: A common cause of persistent infections. *Science* 284(5418):1318–1322.
11. Hall-Stoodley L, Costerton JW, Stoodley P (2004) Bacterial biofilms: From the natural environment to infectious diseases. *Nat Rev Microbiol* 2(2):95–108.
12. Weigel LM, et al. (2007) High-level vancomycin-resistant Staphylococcus aureus isolates associated with a polymicrobial biofilm. *Antimicrob Agents Chemother* 51(1):231–238.
13. Ma H, Bryers JD (2013) Non-invasive determination of conjugative transfer of plasmids bearing antibiotic-resistance genes in biofilm-bound bacteria: Effects of substrate loading and antibiotic selection. *Appl Microbiol Biotechnol* 97(1):317–328.
14. Baddour LM, et al.; American Heart Association Rheumatic Fever, Endocarditis, and Kawasaki Disease Committee; Council on Cardiovascular Disease in Young; Council on Cardiovascular Surgery and Anesthesia; Council on Cardiovascular Nursing; Council on Clinical Cardiology; Interdisciplinary Council on Quality of Care; American Heart Association (2010) Update on cardiovascular implantable electronic device infections and their management: A scientific statement from the American Heart Association. *Circulation* 121(3):458–477.
15. Osmon DR, et al.; Infectious Diseases Society of America (2013) Diagnosis and management of prosthetic joint infection: Clinical practice guidelines by the Infectious Diseases Society of America. *Clin Infect Dis* 56(1):e1–e25.
16. Sandoe JA, et al.; British Society for Antimicrobial Chemotherapy; British Heart Rhythm Society; British Cardiovascular Society; British Heart Valve Society; British Society for Echocardiography (2015) Guidelines for the diagnosis, prevention and management of implantable cardiac electronic device infection. Report of a joint Working Party project on behalf of the British Society for Antimicrobial Chemotherapy (BSAC, host organization), British Heart Rhythm Society (BHRS), British Cardiovascular Society (BCS), British Heart Valve Society (BHVS) and British Society for Echocardiography (BSE). *J Antimicrob Chemother* 70(2):325–359.
17. Greenspon AJ, et al. (2011) 16-year trends in the infection burden for pacemakers and implantable cardioverter-defibrillators in the United States 1993 to 2008. *J Am Coll Cardiol* 58(10):1001–1006.
18. Diefenbeck M, Mückley T, Hofmann GO (2006) Prophylaxis and treatment of implant-related infections by local application of antibiotics. *Injury* 37(Suppl 2):S95–S104.
19. Hake ME, et al. (2015) Local antibiotic therapy strategies in orthopaedic trauma: Practical tips and tricks and review of the literature. *Injury* 46(8):1447–1456.
20. Kang DG, Holekamp TF, Wagner SC, Lehman RA, Jr (2015) Intrasite vancomycin powder for the prevention of surgical site infection in spine surgery: A systematic literature review. *Spine J* 15(4):762–770.
21. ter Boo GJ, Grijpma DW, Moriarty TF, Richards RG, Eglin D (2015) Antimicrobial delivery systems for local infection prophylaxis in orthopedic- and trauma surgery. *Biomaterials* 52:113–125.
22. Campoccia D, Montanaro L, Speziale P, Arciola CR (2010) Antibiotic-loaded biomaterials and the risks for the spread of antibiotic resistance following their prophylactic and therapeutic clinical use. *Biomaterials* 31(25):6363–6377.
23. Lim SH, Mao HQ (2009) Electrospun scaffolds for stem cell engineering. *Adv Drug Deliv Rev* 61(12):1084–1096.
24. Chou SF, Carson D, Woodrow KA (2015) Current strategies for sustaining drug release from electrospun nanofibers. *J Control Release* 220(Pt B):584–591.
25. Dash TK, Konkimalla VB (2012) Poly-ε-caprolactone based formulations for drug delivery and tissue engineering: A review. *J Control Release* 158(1):15–33.
26. Jain RA (2000) The manufacturing techniques of various drug loaded biodegradable poly(lactide-co-glycolide) (PLGA) devices. *Biomaterials* 21(23):2475–2490.
27. Lora-Tamayo J, et al.; REIPI Group for the Study of Prosthetic Infection (2013) A large multicenter study of methicillin-susceptible and methicillin-resistant Staphylococcus aureus prosthetic joint infections managed with implant retention. *Clin Infect Dis* 56(2):182–194.
28. Senneville E, et al. (2011) Outcome and predictors of treatment failure in total hip/knee prosthetic joint infections due to Staphylococcus aureus. *Clin Infect Dis* 53(4):334–340.
29. Liu C, et al.; Infectious Diseases Society of America (2011) Clinical practice guidelines by the Infectious Diseases Society of America for the treatment of methicillin-resistant Staphylococcus aureus infections in adults and children. *Clin Infect Dis* 52(3):e18–e55.
30. Niska JA, et al. (2013) Vancomycin-rifampin combination therapy has enhanced efficacy against an experimental Staphylococcus aureus prosthetic joint infection. *Antimicrob Agents Chemother* 57(10):5080–5086.
31. Pribaz JR, et al. (2012) Mouse model of chronic post-arthroplasty infection: Noninvasive in vivo bioluminescence imaging to monitor bacterial burden for long-term study. *J Orthop Res* 30(3):335–340.
32. Niska JA, et al. (2012) Daptomycin and tigecycline have broader effective dose ranges than vancomycin as prophylaxis against a Staphylococcus aureus surgical implant infection in mice. *Antimicrob Agents Chemother* 56(5):2590–2597.
33. Nishitani K, et al. (2015) Quantifying the natural history of biofilm formation in vivo during the establishment of chronic implant-associated Staphylococcus aureus osteomyelitis in mice to identify critical pathogen and host factors. *J Orthop Res* 33(9):1311–1319.
34. Sridhar R, et al. (2015) Electrosprayed nanoparticles and electrospun nanofibers based on natural materials: Applications in tissue regeneration, drug delivery and pharmaceuticals. *Chem Soc Rev* 44(3):790–814.
35. Son YJ, Kim WJ, Yoo HS (2014) Therapeutic applications of electrospun nanofibers for drug delivery systems. *Arch Pharm Res* 37(1):69–78.
36. LaPlante KL, Mermel LA (2007) In vitro activity of daptomycin and vancomycin lock solutions on staphylococcal biofilms in a central venous catheter model. *Nephrol Dial Transplant* 22(8):2239–2246.
37. Vergidis P, et al. (2011) Treatment with linezolid or vancomycin in combination with rifampin is effective in an animal model of methicillin-resistant Staphylococcus aureus foreign body osteomyelitis. *Antimicrob Agents Chemother* 55(3):1182–1186.
38. Gander S, Hayward K, Finch R (2002) An investigation of the antimicrobial effects of linezolid on bacterial biofilms utilizing an in vitro pharmacokinetic model. *J Antimicrob Chemother* 49(2):301–308.
39. Reipert A, Ehlert K, Kast T, Bierbaum G (2003) Morphological and genetic differences in two isogenic Staphylococcus aureus strains with decreased susceptibilities to vancomycin. *Antimicrob Agents Chemother* 47(2):568–576.
40. Goodman SB, Yao Z, Keeney M, Yang F (2013) The future of biologic coatings for orthopaedic implants. *Biomaterials* 34(13):3174–3183.
41. Fredenberg S, Wahlgren M, Reslow M, Axelsson A (2011) The mechanisms of drug release in poly(lactic-co-glycolic acid)-based drug delivery systems: A review. *Int J Pharm* 415(1–2):34–52.
42. Dash TK, Konkimalla VB (2012) Polymeric modification and its implication in drug delivery: Poly-ε-caprolactone (PCL) as a model polymer. *Mol Pharm* 9(9):2365–2379.
43. Corona PS, et al. (2014) Antibiotic susceptibility in gram-positive chronic joint arthroplasty infections: Increased aminoglycoside resistance rate in patients with prior aminoglycoside-impregnated cement spacer use. *J Arthroplasty* 29(8):1617–1621.
44. Mittal S, et al. (2014) Cardiac implantable electronic device infections: Incidence, risk factors, and the effect of the AigisRx antibacterial envelope. *Heart Rhythm* 11(4):595–601.
45. Kolek MJ, Dresen WF, Wells QS, Ellis CR (2013) Use of an antibacterial envelope is associated with reduced cardiac implantable electronic device infections in high-risk patients. *Pacing Clin Electrophysiol* 36(3):354–361.
46. Bjarnsholt T, Ciofu O, Molin S, Givskov M, Høiby N (2013) Applying insights from biofilm biology to drug development: Can a new approach be developed? *Nat Rev Drug Discov* 12(10):791–808.
47. Campoccia D, Montanaro L, Arciola CR (2013) A review of the biomaterials technologies for infection-resistant surfaces. *Biomaterials* 34(34):8533–8554.
48. Francis KP, et al. (2000) Monitoring bioluminescent Staphylococcus aureus infections in living mice using a novel luxABCDE construct. *Infect Immun* 68(6):3594–3600.
49. Ordonez AA, et al. (2015) Radioiodinated DPA-713 imaging correlates with bactericidal activity of tuberculosis treatments in mice. *Antimicrob Agents Chemother* 59(1):642–649.
50. Hegde SS, Reyes N, Skinner R, Difuntorum S (2008) Efficacy of telavancin in a murine model of pneumonia induced by methicillin-susceptible Staphylococcus aureus. *J Antimicrob Chemother* 61(1):169–172.